Available online at www.sciencedirect.com
SCIENCE DIRECT®
Tectonophysics 370 (2003) 163–176
TECTONOPHYSICS
www.elsevier.com/locate/tecto

Elastic wave velocities and permeability of cracked rocks

Y. Guéguen*, A. Schubnel

Department of Terre Atmosphere Ocean, Ecole Normale Superieure, 24 Rue Lhomond, Paris 74231, France

Accepted 31 March 2003

Abstract

Cracks play a major role in most rocks submitted to crustal conditions. Mechanically, cracks make the rock much more compliant. They also make it much easier for fluid to flow through any rock body. Relying on Fracture Mechanics and Statistical Physics, we introduce a few key concepts, which allow to understand and quantify how cracks do modify both the elastic and transport properties of rocks. The main different schemes, which can be used to derive the elastic effective moduli of a rock, are presented. It is shown from experimental results that an excellent approximation is the so-called non-interactive scheme. The main consequences of the existence of cracks on the elastic waves is the development of elastic anisotropy (due to the anisotropic distribution of crack orientations) and the dispersion effect (due to microscopic local fluid flow). At a larger scale, macroscopic fluid flow takes place through the crack network above the percolation threshold. Two macroscopic fluid flow regimes can be distinguished: the percolative regime close to the percolation threshold and the connected regime well above it. Experimental data on very different rock types show both of these behaviors.

Keywords: Elastic wave; Cracked rocks; Permeability

1. Introduction

The understanding and quantification of rock elastic wave velocities variations is of great interest to extract from seismic and seismological data any information on the physical state of the rock. In the oil industry, this has direct bearings on a quantification of the oil content and the identification of the fluid nature, i.e. oil or gas. In seismotectonics, an open question is to know whether earthquakes can be predicted or not. Elastic wave velocities variations have been considered as a possible precursory effect in that case. Similarly, the understanding and quantification of fluid flow through rocks is a key point for the oil industry, the safety of any underground storage and the possible hydro-mechanical coupling taking place during fault motion. A great amount of data has been obtained on these rock properties by Pr. Kern during the last 20 years (Kern, 1978, 1982; Kern et al., 1997). In crustal conditions, all rocks contain cracks. Cracks represent an extremely small amount of porosity. Yet they have been identified for a long time as a major cause of elastic properties modifications (Simmons and Brace, 1965; Walsh, 1965). Their existence explain the differences observed between static and dynamic moduli, and also the elastic anisotropy of rocks which do not exhibit any mineral preferred orientation (Kern, 1978). When fluids are present,

* Corresponding author. Tel.: +33-144322210; fax: +33-144322200.

0040-1951/03/$ - see front matter © 2003 Elsevier B.V. All rights reserved.
doi:10.1016/S0040-1951(03)00184-7

cracks play another key role: they constitute a network through which fluids can flow at a macroscopic scale, making the rock permeable. This effect has been analysed in terms of percolation theory (Dienes, 1982; Madden, 1983; Rivier et al., 1985) and experimentally observed on various rock types (Fisher and Paterson, 1992; Peach and Spiers, 1996). We present in the following a way to deal with cracks in rocks relying on two well established and fruitful bodies of knowledge, namely Fracture Mechanics and Statistical Physics. We recall first the appropriate results to be used, and apply them successively to the elastic properties and to permeability.

2. How to deal with the damage which results from cracking?

We examine in this section a few key results of Fracture Mechanics and Statistical Physics, which are of interest for our purpose. The following results provide useful tools to deal with damage effects as will be shown later on.

2.1. Crack mechanics

Fracture Mechanics has been developed through the last 50 years at a point which is such that it provides a broad framework to deal with cracks, in particular in the simple case of an elastic behavior. For plane cracks, it is classical to distinguish three basic modes of crack surface displacement: mode I (opening mode), mode II (sliding mode) and mode III (tearing mode). Let us consider a single, traction-free, crack in an isotropic, linear elastic solid, uniformly loaded on its boundary. This situation is equivalent to that of the same solid with traction applied to the crack faces and the solid boundary free, to within a homogeneous stress state. Indeed, the second situation (traction applied to the crack faces, solid boundary free) can be obtained by adding to the first one (traction free crack, solid boundary loaded) an appropriate and identical load on both the external solid boundary and the internal crack face (Fig. 1). The homogeneous stress state corresponding to this last situation is that which would exist if no crack was present.

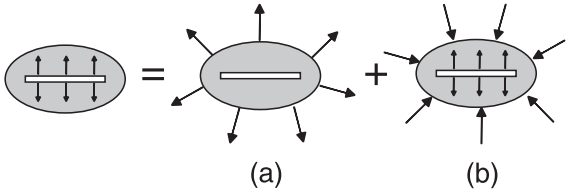

Fig. 1. Loaded crack in an unloaded solid. This situation is equivalent to the superimposition of (a) an unloaded crack in a loaded solid, (b) an identical load applied on both the external surface of the solid and the internal crack faces (case b is an homogeneous stress state, so that everything is "as if" there was no crack).

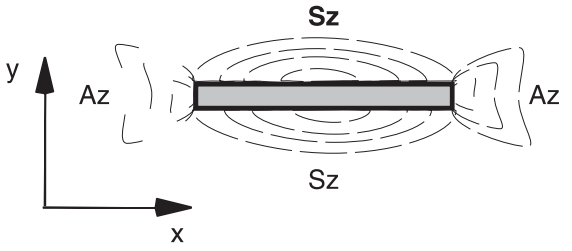

Fig. 2. Stress field σ_{yy} in the case of mode I. Note the existence of a shield zone (Sz) above and below the crack and that of an amplification zone (Az) at the crack tips.

We will concentrate in the following on situations where crack faces are loaded. The stress and displacement fields generated by a loaded crack in a linear elastic solid can be represented by a superposition of the fields produced by modes I, II and III. The solutions are summarized by Kachanov (1993), who pointed an interesting feature of the mode I field in the 2D case (Fig. 2): there exists in that case a region of compressive stress which is rather large above and below the crack, whereas a small tensile region is present at the crack tips. This has important consequences for crack interactions when a population of cracks is considered. If a second crack is placed approximately above a first one, there will be a shielding effect. If it is lined up with the first one, an amplification effect is expected. Since all rocks contain many cracks, such interactions have to be accounted for.

How does a crack affect elastic waves? The stress field of the elastic wave, when applied to the crack faces, produces an additional strain which would not exist in the absence of the crack. In the ideal case that we have considered, this strain is reversible since no friction and no crack propagation are considered. The

existence of the additional strain however means that the elastic stiffness are lower in the cracked rock than in the uncracked rock (or equivalently, the compliances are larger). In order to calculate the additional strain, a preliminary step is to derive the crack opening displacement (also known as displacement discontinuity) $\vec{b}$. The displacement discontinuity is defined as $\vec{b} = \vec{u_1} - \vec{u_2}$, where $\vec{u_1}$ is the displacement vector of a point on the first crack face and $\vec{u_2}$ that of a point on the second crack face. The average additional strain due to a planar crack of surface area S in a sample rock volume V is: $\delta\epsilon_{ij} = 1/2V(\langle b_i\rangle n_j + \langle b_j\rangle n_i)S$, where $\vec{n}$ is the unit normal to the crack and $\langle\vec{b}\rangle$ the average displacement discontinuity at the crack surface. It results that if the crack orientation is known, the extra strain is known and so are the modified stiffness. Following the previous scheme, the way a single crack affects elastic waves is thus relatively easy to quantify. Kachanov (1993) introduced the symmetric second rank crack compliance tensor B_{ij}, which expresses the vector of average displacement discontinuity $\langle b_i\rangle$ in terms of the uniform traction $\vec{t}$ applied to the crack faces: $\langle b_i\rangle = B_{ip}t_p$. The tensor B_{ip} is known for circular (and elliptical) cracks in the 3D case. Then using $t_p = \sigma_{pq}n_q$, one gets: $\delta\epsilon_{ij} = 1/2V(B_{ip}\sigma_{pq}n_q n_j + B_{jp}\sigma_{pq}n_q n_i)S$. The extra strain can also be written in terms of the extra compliances:

$$\delta S_{ijkl} = \frac{S}{4V}(B_{ik}n_l n_j + B_{il}n_k n_j + B_{jk}n_l n_i + B_{jl}n_k n_i) \tag{1}$$

The increase in compliances correspond to a decrease in stiffness, from which the velocity decrease is obtained. The crack compliance tensor can be expressed as a sum of a normal, B_N, and shear, B_T, term (Sayers and Kachanov, 1995): $B_{ij} = B_N n_i n_j + B_T(\delta_{ij} - n_i n_j)$. We will consider later on penny shaped cracks with radius c. In that case, if E is the rock Young modulus and ν its Poisson ratio, $B_T = (32(1-\nu^2)c)/(3\pi E(2-\nu))$ and $B_N/B_T = 1 - (\nu/2)$ for dry cracks, or $B_N/B_T = 1 - (\nu/2)(\delta/1+\delta)$ for fluid saturated cracks (Kachanov, 1993). The above results are valid for an isotropic elastic solid, which is the situation we are interested in. The parameter δ characterizes the coupling between the stress and the fluid pressure:

$$\delta = \beta^{-1}\frac{E\zeta}{K_f} \tag{2}$$

where E is the intact rock Young modulus, K_f the fluid bulk modulus, ζ the crack aspect ratio ($\zeta = w/c$ where w is the crack aperture) and β is a numerical factor such as $\beta = 16(1-\nu^2)/3\pi$. Relying on the above results, it is then possible to quantify the effects of a population of cracks within various approximations as examined in Section 3. In order to derive the modified compliance in a realistic case, the previous results on a single crack constitute a necessary, but not sufficient step. As far as the elastic properties are concerned, extrapolating from a single crack to a population of cracks is not straightforward. How to account for crack interactions? This question points to effective media theories, which will be considered in Section 3.

2.2. Statistical physics

Another important question examined in this paper is: how does a population of cracks modify the rock permeability? Statistical Physics allows us to address in a simple way that question because—through percolation theory—it is the appropriate tool to quantify the connectivity issue. Fluid flow through a planar single crack is a well-known process which is quantitatively described by Poiseuille law, at least if roughness effects are negligible. A cracked rock will have however a zero permeability as long as the cracks do not form a connected network. Connection occurs at a threshold called the percolation threshold. Percolation theory provides a framework to calculate this threshold (Stauffer and Aharony, 1992). Percolation has been mainly investigated on regular geometric networks. In such cases, cracks are considered as bonds, which are randomly distributed over a periodic 2D or 3D network. A key parameter is the probability p for a bond to be occupied by a crack. The percolation threshold is reached at a critical value p_c, which depends on the network geometry. For instance, $p_c = 0.5$ for bond percolation on a 2D square lattice and $p_c = 0.18$ for bond percolation on a 3D bcc lattice. In real rocks, however, cracks are distributed continuously through the 3D space. In order to take into account this fact, it is useful to introduce the statistical concept of excluded volume (De Gennes, 1976). The excluded volume V_e is the average volume around one object (here a penny shaped crack) within which a second similar object must have its center in order for the two objects to intersect. In the case of a penny shaped crack

of radius c, $V_e = \pi^2 c^3$ (De Gennes, 1976). Assuming a homogeneous distribution of N cracks per unit volume, one can show that $p \approx \pi^2/4Nc^3$ (Guéguen and Dienes, 1989) for a coordination number of 4 (i.e. in average each crack has 4 neighbors). Assuming also a value of 1/3 for p_c, one sees that the percolation threshold is expected for a critical value of the quantity Nc^3 such as $Nc^3 = 0.13$. As will be seen in Section 3, the quantity Nc^3 is a key parameter for both the elastic properties and permeability. Let us point out that it is the simplest nondimensional quantity, which can be constructed from N and c. The value of 0.13 should be regarded as an approximate value because of the approximations which have been made. It is clear however that there are two distinct regimes to be considered, depending on whether or not $Nc^3 \leq 0.1$. Below the percolation threshold, the overall permeability is zero (no crack connection).

3. Elastic wave velocities

Because the elastic moduli values decrease when cracks are present, as explained in Section 2, the elastic wave velocities are also expected to decrease. Since any velocity is expressed in terms of some modulus M and density ρ by $V = (M/\rho)^{0.5}$, and because the crack porosity is so small that the ρ decrease induced by cracking is much less than the M decrease, such a behavior is simple to understand. However two other important effects will take place as well: the development of anisotropy and, if the rock is fluid saturated, dispersion. Before investigating these effects, it is necessary to extend the results established in Section 2 for a single crack to the case of a population of cracks.

3.1. Effective media theories: approximate schemes for calculating compliances

To extend the results obtained for a single crack requires to address the issue of crack interactions. Calculating exactly the interactions of a population of many cracks is a very difficult task. As shown below, there exist however some simple and efficient ways to get around this difficulty. This can be approximately done by using Effective Media Theories (EMT). Two different approaches can be used in EMT calculations. One is the approximation of an effective matrix, the other the approximation of an effective field. In the first case, each crack is assumed to be isolated in a medium, which is the effective matrix. The properties of this matrix are calculated to take approximately into account crack interactions. The calculations follow then the scheme presented in Section 2 for an isolated crack. In the second case, crack interactions are accounted for through an effective stress, which is not the applied stress but the applied stress modified by the presence of cracks.

A detailed overview of the results relative to effective elastic properties of cracked solids has been given by Kachanov (1992,1993). Of special interest is the model of *noninteracting* cracks. As shown by Kachanov, this model remains accurate at high cracks densities, provided the *location of crack centers are at random*. It is an effective matrix model; the simplest one indeed since the matrix is assumed to be the intact rock. We give below the results of this model because of their broad range of validity and their broad field of application. There are in fact two different ways of understanding why it is so. At a microscopic level, crack interactions exist but compensate approximately. The shielding and amplification effects examined in Section 2 cancel each other in average. At a macroscopic level, the effective stress can be approximately taken as the volumetric averaged field. But it is a well-established result that the volumetric averaged stress field is not modified by the presence of cracks. The simplest effective stress model leads thus also to the non-interacting crack model.

3.2. Anisotropy and crack density

We adopt in the following the non-interacting scheme in order to calculate the elastic compliances and hence the elastic wave velocities in terms of crack density. The cracks are assumed to be identical, disc shaped, with a radius c. The results of Section 3.1 give the extra compliances in terms of the tensor B_{ij} and the values of the B_{ij} components. Assuming an homogeneous distribution of N cracks per unit volume, the extra compliances can be written as:

$$\delta S_{ijkl} = \pi N c^2 \left[\frac{B_T}{4} \langle (\delta_{ik} n_j n_l + \delta_{il} n_j n_k + \delta_{jk} n_i n_l + \delta_{jl} n_i n_k) \rangle + (B_N - B_T) \langle n_i n_j n_k n_l \rangle \right] \quad (3)$$

Let us introduce the normalizing factor h such as:

$$h = \frac{3E(2-\nu)}{32(1-\nu^2)} \tag{4}$$

Then Eq. (3) is modified into:

$$\delta S_{ijkl} = \frac{Nc^3}{h}\left[\frac{1}{4}\langle(\delta_{ik}n_jn_l + \delta_{il}n_jn_k + \delta_{jk}n_in_l + \delta_{jl}n_in_k)\rangle + \left(\left(1-\frac{\nu}{2}\right)\frac{\delta}{1+\delta} - 1\right)\langle n_in_jn_kn_l\rangle\right]$$

Following Sayers and Kachanov (1991, 1995) and Schubnel et al. (2003), let us define the second rank tensor $\alpha^*_{ij} = Nc^3\langle n_in_j\rangle$, which is the crack density tensor. We note that $tr\alpha^* = \alpha^*_{kk} = Nc^3$. This last quantity is a key parameter for crack connectivity as shown in Section 2. Let us define also a fourth rank tensor $\beta^*_{ijkl} = Nc^3((B_N/B_T) - 1)\langle n_in_jn_kn_l\rangle$, which is $\beta^*_{ijkl} = Nc^3[(1-(\nu/2))(\delta/(1+\delta)) - 1]\langle n_in_jn_kn_l\rangle$. These tensors represent respectively the second order moment and 4th order moment of the crack orientation distribution function. We will use the following notations:

$$\alpha^*_{ij} = (tr\alpha^*)\langle n_in_j\rangle \tag{6}$$

$$\beta^*_{ijkl} = \left[\left(1-\frac{\nu}{2}\right)\frac{\delta}{1+\delta} - 1\right](tr\alpha^*)\langle n_in_jn_kn_l\rangle \tag{7}$$

Then the extra compliance tensor is expressed as:

$$\delta S_{ijkl} = \frac{1}{h}\left[\frac{1}{4}(\delta_{ik}\alpha^*_{jl} + \delta_{il}\alpha^*_{jk} + \delta_{jk}\alpha^*_{il} + \delta_{jl}\alpha^*_{ik}) + \beta^*_{ijkl}\right] \tag{8}$$

For simplicity, we now assume that the anisotropy is of the transversely isotropic type (hexagonal symmetry). Indeed, any more complex symmetry would be very difficult to deal with for practical reasons. The transversely isotropic symmetry corresponds to five independent elastic constants and the next step in increasing complexity involves nine independent elastic constants (orthorhombic symmetry). The definitions of both tensors α^* and β^*, together with the relation $2\delta S_{1212} = (\delta S_{1111} - \delta S_{1122})$ imposed by the choice of a transversely isotropic symmetry (Nye, 1979), lead to the following relations:

$$\delta S_{1111} = \delta S_{2222} = \frac{1}{h}(\alpha^*_{11} + \beta^*_{1111})$$

$$\delta S_{3333} = \frac{1}{h}(\alpha^*_{33} + \beta^*_{3333})$$

$$\delta S_{1212} = \frac{1}{h}\left(\frac{\alpha^*_{11}}{2} + \frac{\beta^*_{1111}}{3}\right)$$

$$\delta S_{2323} = \delta S_{3131} = \frac{1}{h}\left(\frac{\alpha^*_{11} + \alpha^*_{33}}{4} + \beta^*_{1133}\right)$$

$$\delta S_{1122} = \frac{1}{h}\left(\frac{\beta^*_{1111}}{3}\right)$$

$$\delta S_{2233} = \delta S_{3311} = \frac{1}{h}\beta^*_{1133} \tag{9}$$

The set of Eqs. (2), (4), (6), (7) and (9) allow to calculate the cracked rock elastic compliances, and hence wave velocities, in terms of three material parameters of the intact rock and of the fluid: ν, E, K_f, one geometrical crack parameter ζ and the two crack density tensors α^* and β^*. The five independent elastic constants of the transversely isotropic symmetry correspond to the five components α^*_{11}, α^*_{33}, β^*_{1111}, β^*_{3333} and β^*_{1133} of the second and fourth order crack density tensors. These last five parameters depend only on the crack orientation distribution function. It is thus possible to predict and quantify the elastic anisotropy if the crack orientation distribution function is known. Alternatively, it is possible to extract from elastic wave velocities data the crack orientation distribution function. An interesting point is that we can discriminate between dry and saturated cracks because in the first case $K_f = 0$ and $\delta \to \infty$, whereas in the second one $K_f \gg 0$ and $\delta \approx 0$. More precisely, these two possibilities correspond to two values of the β^* tensor, which can be summarized as:

$$\beta^*_{ijkl} = -\gamma\ tr\alpha^*\langle n_in_jn_kn_l\rangle \text{ with } \gamma = \frac{\nu}{2} \text{ (dry) or } \gamma = 1 \text{ (saturated)} \tag{10}$$

The previous model was checked against experimental data in two very different cases, one corresponding to a dry sandstone (Scott et al., 1993) and the other to a saturated granite (Schubnel et al., 2003). The first case was previously discussed by Sayers and Kachanov (1995) who have shown that the β^* values are negligible in the dry case. In agreement with Eq. (10): with $\nu \simeq 0.14$ and $\gamma = \nu/2$, the β^* values are at least one order of magnitude lower than the α^* values (in the dry case), and crack density tensor components can be extracted with reasonable confidence from a set of four independent elastic velocities. Fig. 3a and b shows velocity measurements performed by Scott et al. (1993) on a dry Berea sandstone sample at 20 MPa confining pressure and the crack density as inferred form those measurements by Sayers and Kachanov (1995), respectively. During this experiment, P velocities were measured along the vertical axis (referred as 3 here) and the horizontal one. Transverse isotropy was assumed so that horizontal axis 1 and 2 were equivalent. On Fig. 3a, V_{ij} refers to the wave propagating parallel to axis i and vibrating along axis j. V_{33} is therefore the P wave propagating along the vertical axis of the sample, whereas V_{12} the horizontal shear wave propagating in the horizontal plane. One should note on Fig. 3a that P wave anisotropy and S wave birefringence is shear enhanced as the differential stress increase, which is certainly the result of crack nucleation and propagation (i.e. crack density increase). Results on Fig. 3b show that during such a triaxial compression test, total crack density ($tr(\alpha^*) = 2\alpha^*_{11} + \alpha^*_{22}$) actually increases at the onset of dilatancy and reaches a total value close to 1 near rupture (in the brittle regime). Elastic wave anisotropy can thus be interpreted as a crack density anisotropy, since the total vertical crack density ($\alpha^*_{11} + \alpha^*_{22}$ for a transversely isotropic medium) show a significant increase compared to the horizontal crack density that remains more or less constant. Let us point out that, in their analysis, Sayers and Kachanov considered the whole range of experiments performed at confining pressure of 20, 60 and 138 MPa on dry Berea sandstone

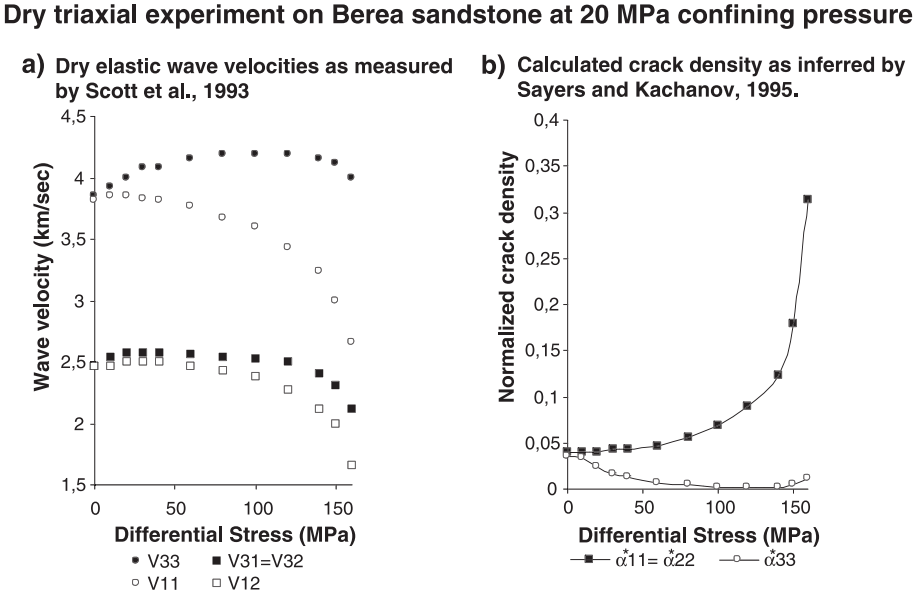

Fig. 3. Dry triaxial experiment on Berea sandstone at 20 MPa confining pressure. (a) Ultrasonic wave velocities for propagation parallel and perpendicular to the maximum compressive stress measured by Scott et al. (1993). The velocities plotted are V33 (plain circles), V11 (open circles), V31 and V32 (plain squares) and V12 (open squares) in the coordinate system defined in this paper with Ox_3 parallel to the maximum compressive stress. (b) Components $\alpha^*_{11} = \alpha^*_{22} =$ (solid squares) and α^*_{33} of the crack density tensor obtained by Sayers and Kachanov (1995) when inverting the wave velocities shown on (a).

by Scott et al. (1993). They noted that the samples loaded at 20 and 60 MPa exhibit dilatancy prior to failure, whereas the sample loaded at 138 MPa confining pressure exhibited inelastic compaction. It is clear that at higher confining pressure, brittle behavior and dilatancy enter in competition with compaction and cataclastic flow in a porous sandstone. These effects have been thoroughly investigated by Wong et al. (1997). In such cases, a simple crack analysis like the following one cannot take into account the porosity reduction that also affects elastic wave velocities.

The second case that we consider is the saturated one, $\gamma = 1$, so that the β^* values are not negligible, and all five α^*_{11}, α^*_{33}, β^*_{1111}, β^*_{3333} and β^*_{1133} constants should be extracted from at least five independent velocity paths. Fig. 4 shows elastic wave velocity measurements obtained during a wet triaxial compression test on Oshima granite (Schubnel et al., 2003). The confining pressure was equal to 40 MPa and the pore pressure to 10 MPa. Fig. 4a–c shows P, SV and SH waves velocity measurements respectively. All velocities increase as the confining pressure is raised up to 40 MPa. Vertical anisotropy becomes lower than 10% as the cracks are being closed with effective mean stress. In the intermediate range of effective pressure, horizontal anisotropy becomes almost negligible and the sample fits a transverse isotropy. The onset of dilatancy C' is reached at a critical value of effective mean stress and, beyond C', horizontal and diagonal velocities decrease because of crack growth and propagation. Vertically measured P velocity stays nearly constant, which suggests that most of the stress-induced microcracks are vertical, and thus invisible to vertical P wave. This corresponds also to an increase in the acoustic emission rate. Fig. 4d shows the crack density α^* and β^* components as inferred from those velocity measurements. An increase in crack density occurs when C' is reached, the vertical component α_{11} increasing faster. Total crack density $tr(\alpha^*) = 2\alpha^*_{11} + \alpha^*_{33}$ is larger than 1 at failure. The components of the tensor β are negative and diagonal terms β_{1111} and β_{3333} turn out to become large close to failure as expected in the wet case from Eq. (10). In this experiment on a compact rock, no compaction can occur and the crack effect is not blurred by other effects like in a porous sandstone.

To conclude this section, it is interesting to compare Sayers and Kachanov's (1991, 1995) model to several previous models which have been frequently used. Such a comparison can be found also in Kachanov (1993). Hudson (1980, 1981, 1986) developed a dynamic theory considering long wavelength scattered waves and using a pertubation analysis. From Eshelby (1957) results, he obtained the elastic constants for dry and saturated cracks. Anderson et al. (1974), Soga et al. (1978) and Ayling et al. (1995) models follow the same lines. However, an important distinction is not accounted for in those models. If a rock contains cracks of various orientations, or cracks and equant pores (both of these situations are certainly the most common ones) local flow (also called squirt flow) takes place below a certain frequency (O'Connell and Budiansky, 1977). Then a major distinction should be introduced between the two following cases: low frequency (i.e. local isobaric state for the fluid in pores and cracks) and high frequency (i.e. variable fluid pressure from crack to crack). In addition, the case of dry cracks can also be considered. This frequency effect will be examined further in Section 3. The above mentioned models only apply to either the dry case or the saturated high frequency case. They are not valid for the saturated low frequency case, which turns out to be the most important one for field data. On the other hand, the great advantage of the present model is that:

(1) It is directly derived from the elastic potential energy analysis of the rock and therefore relies on a clear micromechanical analysis.
(2) It permits a simple derivation of elastic moduli for any crack and fluid distribution.
(3) It enables us to take into account any kind of fluid in any kind of situation (drained, undrained or high frequency wet response of the rock as we will see in Section 3.3).

3.3. Frequency effects

The low frequency compliances of the saturated cracked rock $(S_{ijkl})_u$ can be related to the drained cracked rock compliances S_{ijkl} and the α, β tensors using the above relations and the Brown–Korringa equations (Brown and Korringa, 1975). The low frequency compliances are indeed equal to the undrained compliances of the poroelastic theory, and

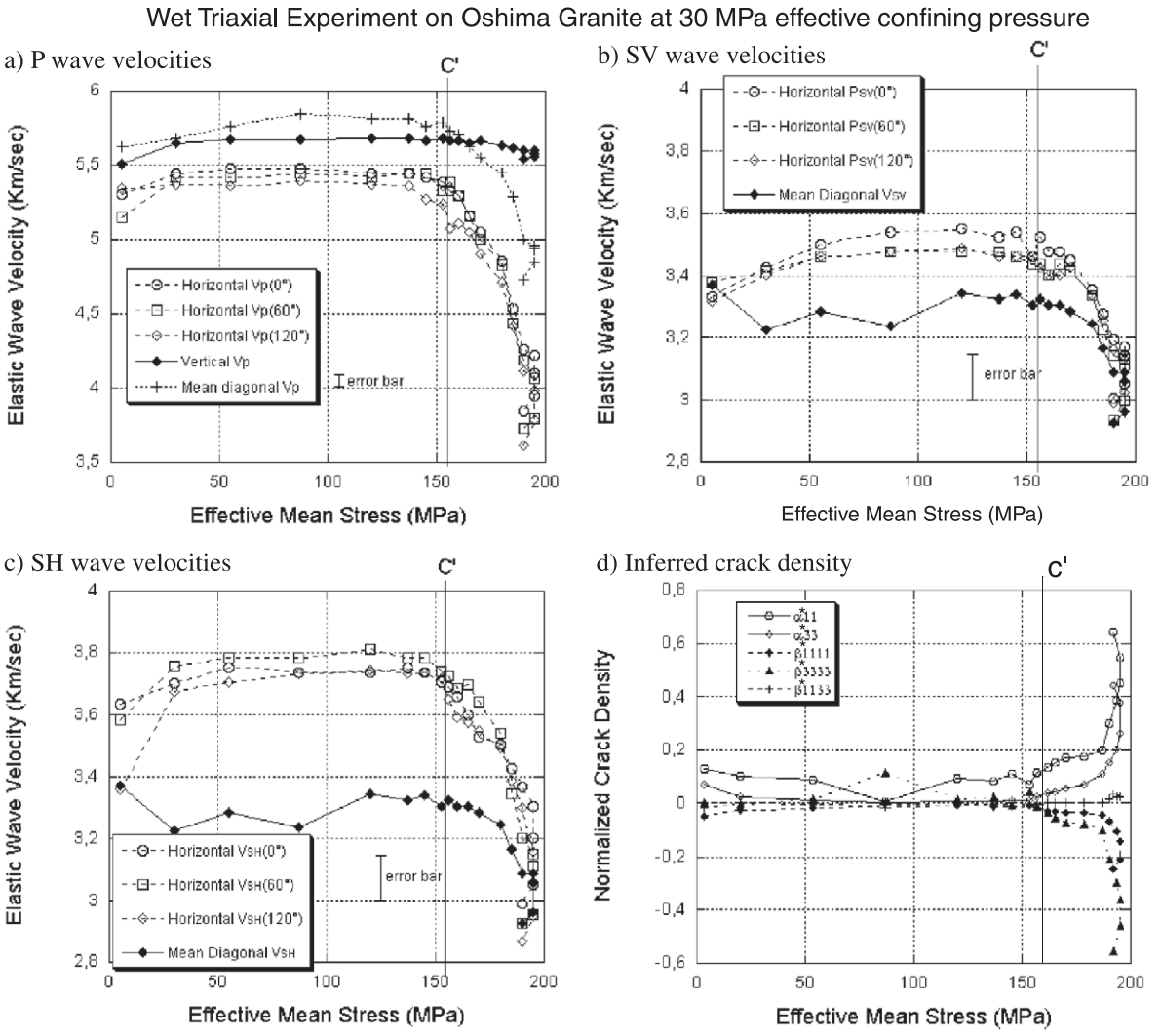

Fig. 4. Wet triaxial experiment on Oshima granite at 30 MPa effective confining pressure. Confining pressure σ_3 was equal to 40 MPa and pore pressure P_p equal to 10 MPa. (a) shows P wave velocities measurements versus effective mean stress $P'=[(\sigma_1+2\sigma_3)/3-P_p]$. Error bar on P wave measurements is ± 0.1 km/s. Plain diamonds show vertical P wave velocity, crosses, mean diagonal P velocity. Open circles, squares and diamonds show horizontal P wave at 0°, 60° and 120° from reference plane respectively. (b) and (c) show SV and SH wave velocities respectively. Error bar on S wave measurements is ± 0.15 km/s. Plain diamonds show mean diagonal S velocity. Open circles, squares and diamonds show horizontal S wave at 0°, 60° and 120° from reference plane, respectively. (d) shows the normalized crack density tensors α^*_{ij} and β^*_{ijkl} versus effective mean stress as inferred from those velocity measurements. α^*_{11} represents the vertical crack density tensor component. Total crack density is equal to $tr(\alpha^*_{ij})$.

the drained compliances are equal to the dry ones. The Brown–Korringa equations are:

$$S_{ijkl}-(S_{ijkl})_u=\frac{[(S_{ijmm}-(S_{ijnn})_s][S_{klpp}-(S_{klqq})_s]}{\frac{1}{K}-\frac{1}{K_s}+\phi_0\left(\frac{1}{K_f}-\frac{1}{K_s}\right)} \tag{11}$$

where the $(S_{ijkl})_s$ are the uncracked rock compliances, K_f and K_s are respectively the fluid and solid phase bulk moduli, ϕ_0 is the rock porosity. Let us point out that, if we consider an isotropic elastic solid matrix, only two independent $(S_{ijkl})_s$ have non-zero values and Eq. (11) is similar to the Biot–Gassman relation

(Gassmann, 1951; Biot 1956a,b). In the general anisotropic case, using Eq. (8) and neglecting the β components for the dry case, Brown and Korringa (1975) equations become:

$$S^{lf}_{ijkl} = (S_{ijkl})_u = (S_{ijkl})_s + \frac{1}{h}\left[\frac{1}{4}(\delta_{ik}\alpha^*_{jl} + \delta_{il}\alpha^*_{jk} + \delta_{jk}\alpha^*_{il} + \delta_{jl}\alpha^*_{ik})\right] - \frac{1}{h^2}\frac{\alpha^*_{ij}\alpha^*_{kl}}{\frac{tr\alpha^*}{h} + \phi_0\left(\frac{1}{K_f} - \frac{1}{K_s}\right)}$$

The high frequency compliances are obtained from Eq. (8) without neglecting the β components, so that:

$$S^{hf}_{ijkl} = (S_{ijkl})_s + \frac{1}{h}\left[\frac{1}{4}(\delta_{ik}\alpha^*_{jl} + \delta_{il}\alpha^*_{jk} + \delta_{jk}\alpha^*_{il} + \delta_{jl}\alpha^*_{ik}) + \beta^*_{ijkl}\right] \quad (13)$$

Then it results that the differences between the high and low frequency compliances are given by:

$$S^{hf}_{ijkl} - S^{lf}_{ijkl} = \frac{1}{h}\left[\beta^*_{ijkl} - \frac{\alpha^*_{ij}\alpha^*_{kl}}{tr\alpha^* + h\phi_0\left(\frac{1}{K_f} - \frac{1}{K_s}\right)}\right] \quad (14)$$

In the above equation, the β components are calculated with $\gamma = 1$. Recalling that $E = 3K_s(1-2\nu)$, h can be expressed in Eq. (14) in terms of K_s and ν. Then we get:

$$\frac{1}{h} = \frac{32(1-\nu^2)}{9(1-2\nu)(2-\nu)}\frac{1}{K_s} \quad (15)$$

so that the difference between high and low frequency velocities depend only on the crack density tensors, the (uncracked) solid and fluid elastic moduli, and the porosity. The elastic wave velocity anisotropy is thus found to depend on the frequency in general. The low frequency limit corresponds to a situation where fluid pressure is equilibrated in pores and cracks. This is no longer true at high frequencies, a situation that is in particular that of laboratory measurements. This frequency dependent behavior produces a dispersion, which was experimentally observed in isotropic media and generally called "squirt flow" mechanism (Mavko and Nur, 1975; O'Connell and Budiansky, 1974, 1977; Thomsen, 1985). Accounting for this effect is of primary importance to interpret seismic data and/or to extrapolate laboratory elastic wave velocities measurements. Typically, the theoretical cutoff frequency is of the order of $f_c = \zeta_o^3 E_o/24\eta$ (Le Ravalec et al., 1996) where ζ_o is the aspect ratio of the crack, E_o the intact rock Young modulus and η the fluid viscosity. For example, assuming $\zeta_o = 10^{-3}$, $E_o = 75$ GPa, $\eta = 10^{-3}$ Pa s^{-1} the cutoff frequency is equal to $f_c \sim 3$ kHz.

In the case of isotropic rocks, models (Mavko and Jizba, 1991; Le Ravalec and Guéguen, 1996) suggest that a small density of cracks may result in a quite large dispersion of the seismic wave velocities. However, most of cracked rocks are found, experimentally, to be seismically anisotropic. Fig. 5 shows numerically predicted dispersion obtained for two different transversely isotropic distributions of cracks (Schubnel and Guéguen, 2003). The propagation angle γ is that between the vertical axis and the wave vector. Dispersion was calculated from: $\text{Disp} = (V^{HF}(\gamma) - V^{LF}(\gamma))/V^{HF}(\gamma) \times 100$ and results are shown for crack densities equal to 0.1, 0.25, 0.5 and 1. The first case (Fig. 5a and b) corresponds to a distribution of horizontally aligned cracks. The dispersion on P wave (Fig. 5a) can be as high 30% for waves propagating along the axis of symmetry and is negligible in the horizontal plane of the rock. Maximum SV wave dispersion (Fig. 5b) is observed for wave propagating along a vector at $\sim 50°$ with the vertical. Let us point out that for such distribution, as intuitively expected, SH waves show no dispersion. The second distribution we considered (Fig. 5c and d) corresponds to that of vertical cracks in zone around the vertical axis (symmetry on ϕ). In such case, dispersion on P wave (Fig. 5c) and on SH wave (Fig. 5d) is maximum in the horizontal plane. Though maximum dispersion should be smaller than

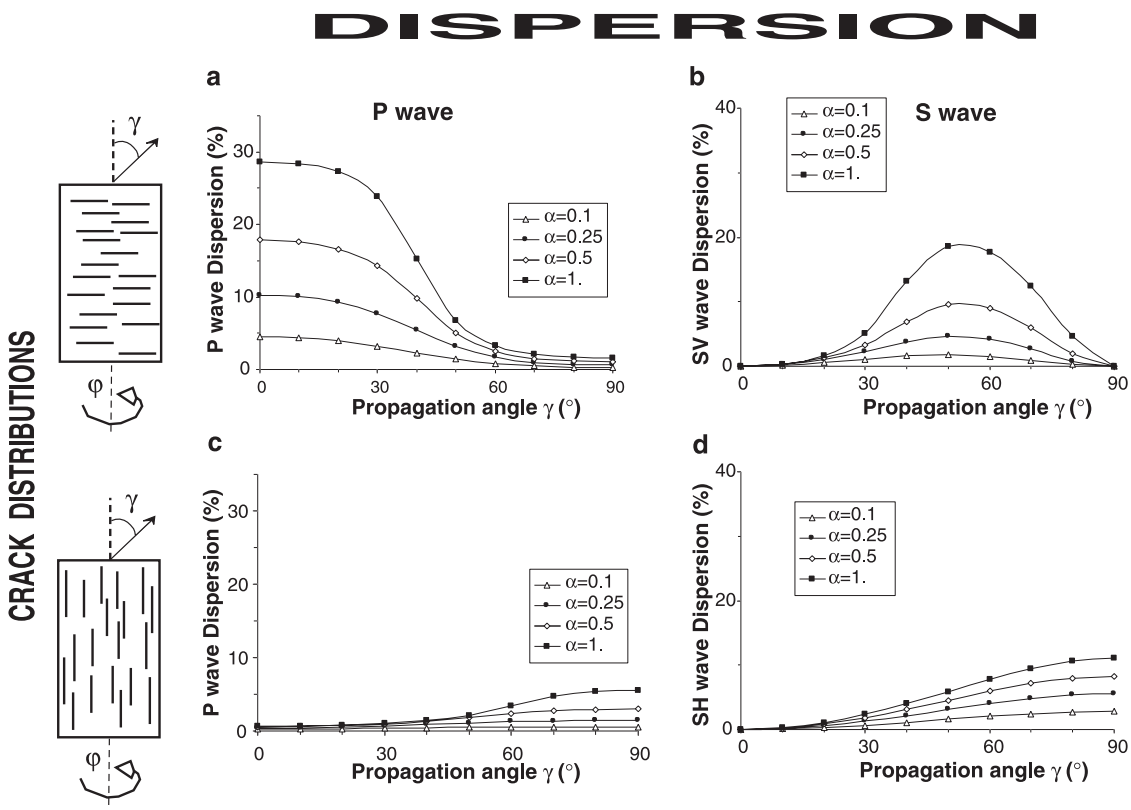

Fig. 5. S wave dispersion for two different distribution of cracks. The first case (a and b) corresponds to a distribution of horizontally aligned cracks. The second distribution (c and d) corresponds to that of vertical cracks in zone around the vertical axis (symmetry on ϕ). Results were obtained for a Young's modulus equal to 75 GPa, a Poisson ratio of 0.25 and an average aspect ratio ζ_0 equal to 0.01. Results are displayed for crack densities equal to 0.1 (open triangles), 0.25 (plain circles), 0.5 (open diamonds) and 1 (plain squares). (a) and (b) show P and SV wave dispersion versus the wave propagation angle γ, respectively, in the case of horizontally aligned cracks. NB: In the case of horizontally aligned cracks, SH waves show no dispersion. (c) and (d) show the P and SH wave dispersion versus the wave propagation angle γ, respectively, in the case of symmetrically aligned vertical cracks (symmetry around the vertical axis, cracks normal in the horizontal axis). NB: In the case of symmetrically aligned vertical cracks, SV waves show no dispersion.

15%. For such distribution of cracks, SV waves show no dispersion, as expected.

4. Permeability

The development of a crack network modifies strongly the rock permeability. Following Dienes (1982) and Guéguen and Dienes (1989), the permeability of a cracked rock in the isotropic case and for penny shaped cracks can be written as:

$$k = \frac{4\pi^2}{15}\zeta^3 N c^5 f \tag{16}$$

where ζ is as above the crack aspect ratio ($\zeta = w/c$), N the number of cracks per unit volume, c the crack radius and f the fraction of cracks which are hydraulically connected.

Although the above result is not relevant for the anisotropic case, it can be extended to it. This result allows us however to separate two main regimes: the percolative regime and the connected regime.

4.1. Percolative regime

As recalled in Section 2, the percolation threshold for a distribution of cracks is expected to be reached for a value of the quantity $tr\alpha^* = Nc^3$ such as

$tr\alpha^* = 0.1$. Below this threshold, the crack system is not connected and the permeability is 0. Using the Bethe lattice model, Guéguen and Dienes (1989) have shown that f could be approximated by:

$$f \simeq \frac{9}{4}\left(p - \frac{1}{3}\right)^2 \quad \text{for} \quad \frac{1}{3} < p < 1 \tag{17}$$

where $p = \pi^2/4Nc^3$ is the probability for two cracks to intersect, with $Nc^3 = tr\alpha^*$. Note that $f = 0$ when $p < 1/3$ and $f = 1$ when $p > 1$. At low crack densities, the permeability is thus zero. When crack nucleation and/or propagation takes place, the connectivity takes a positive non-zero value at the percolation threshold and then increases progressively up to 1 when all cracks are connected (excluding dead ends). The behavior, which is predicted for permeability, is shown on Fig. 6. This behavior is typical of percolation and was obtained as well by many different models (Frisch et al., 1962; Stauffer and Aharony, 1992). It is of interest to compare Fig. 6 to some experimental results. It appears that permeability increases by several orders of magnitude in the percolative regime. Results on granite (Brace et al., 1968), synthetic fine grained halite (Peach and Spiers, 1996) and Carrara marble (Fisher and Paterson, 1992; Zhang et al., 1994) agree with these predictions (Fig. 7), as shown by Zhu and Wong (1999). More specifically, Fig. 7 shows experimental results of k variation with uniaxial strain. Cracking is involved in the deformation regime so that strain is linked with either crack density N or crack length c changes, or both. The experimentally observed increase in k reflects these changes. Since the connectivity factor f depends on N and c as well, f increases strongly up to the point where the overall crack network is well connected (nb: f close to 1 on Fig. 6).

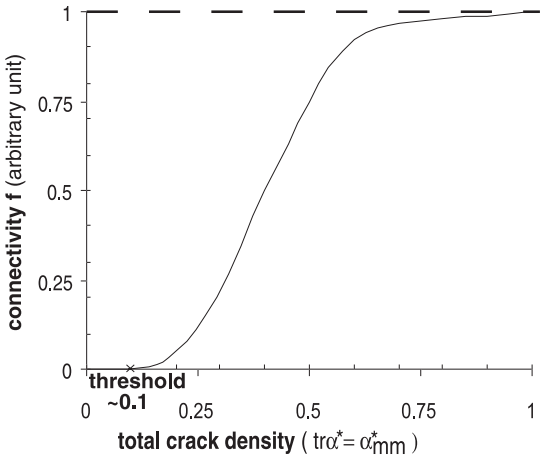

Fig. 6. Connectivity as a function of crack density $tr\alpha^*$. Below the percolation threshold, the connectivity, and hence the permeability is 0. At high crack density values, connectivity is 1.

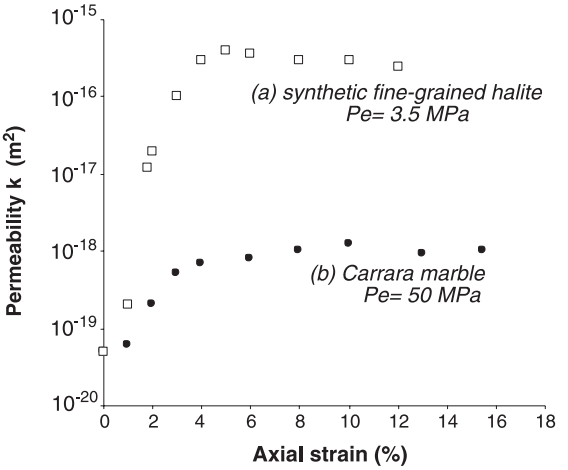

Fig. 7. Experimental data of permeability changes on (a) synthetic fine grained halite (Peach and Spiers, 1996) and (b) Carrara marble (Zhang et al., 1994).

4.2. Connected regime

Above the percolation threshold, connectivity increases up to 1. Further increase in permeability is however possible due to the nucleation and/or propagation of dilatant microcracks, as expected from Eq. (16) since the value of the parameters N and c increases. Dilatancy is produced by the induced wing cracks and also by frictional sliding on rough crack surfaces (Kachanov, 1982). In this connected regime, Simpson et al. (2001) have calculated the evolution of the full permeability tensor by coupling the Kachanov (1982) model with the statistically based Dienes (1982) model, which enables calculation of permeability in anisotropic cracked media. Numerical predictions of the model are in quantitative agreement with published experimental results, which show a moderate permeability increase (factors of 3–4) in this regime (Zoback and Byerlee, 1975). However, in

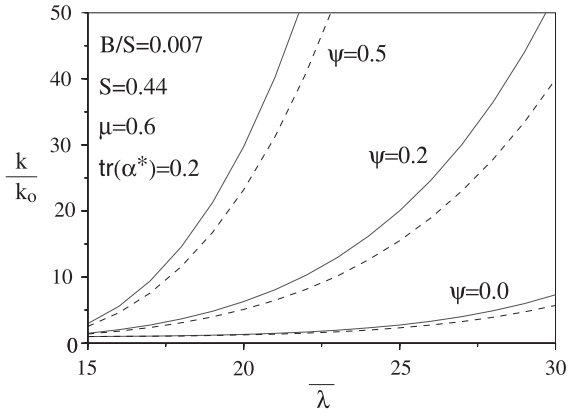

Fig. 8. Normalized permeability in the maximum compression direction σ_1 (solid line) and in the direction of minimum compression σ_3 (dashed line), as predicted by Simpson et al. (2001) in the connected, damage regime. Permeability k_0 is the initial granite permeability for $\lambda=0$ ($k_0 \sim 10^{-19}$ m^{-2}). The crack density value is $tr\alpha^*=0.2$. Permeability is plotted as a function of the effective stress ratio $\bar{\lambda}=(\sigma_1+p_f)/(\sigma_3+p_f)$, where p_f is the pore fluid pressure. The roughness parameter ψ is equal to 0, 0.2 or 0.5.

order to achieve agreement with realistic crack densities, additional dilatancy due to frictional sliding on rough cracks surfaces should be taken into account. Although the permeability is the greatest in the direction of the maximum compressive stress σ_1, permeability anisotropy is relatively small (<10) for anticipated effective stress ratios and friction coefficients. Fig. 8 shows the predicted behavior for an initial crack density value $tr(\alpha^*)$ of 0.2, i.e. just above the percolation threshold. The calculation has been done assuming a roughness parameter of 0, 0.2 and 0.5. The friction coefficient was equal to 0.6. This means that, when the original shear cracks slide past each other, they undergo an additional separation due to uplifting at asperities on the crack surface. The separation w is assumed to be linearly proportional to the amount of sliding u (i.e., $w=\psi u$ where ψ is the roughness parameter). When $\psi=0$, the wing crack still dilates but the relatively small increase in aperture is not sufficient to explain the permeability enhancement observed experimentally. The model involves also other elastic and material parameters. The results depend specifically on two quantities B and S such that $S=-\sigma_3(\pi l_0)^{0.5}/K_{Ic}$ and $B=-\sigma_3(2\pi)^{0.5}(1-\nu^2)/E$. K_{Ic} is the fracture toughness, l_0 is the half length of the original shear cracks, E is the Young modulus and ν the Poisson's ratio. The results in Fig. 8 correspond to $S=0.44$ and $B/S=7\times10^{-3}$.

5. Conclusions

Fracture mechanics and statistical physics have been shown to be two key tools to deal with crack damage in rocks. Effective elastic properties of dry and saturated cracked rocks can be derived up to high crack densities. An important result is that it is possible to express the elastic compliances in terms of the crack density tensor and the intact rock and fluid properties. The results show that the elastic rock anisotropy is directly given in terms of the crack density tensor components. Moreover, high and low frequency elastic wave velocities can differ up to 30% in saturated cracked rocks at high crack densities. The implication is that it is not possible to extrapolate laboratory (high frequency) data to in situ (low frequency) situations. Total crack densities $tr(\alpha^*)$ cover the range 0–1.5. Macroscopic fracture appear at $tr(\alpha^*)$ values between 1 and 1.5. However, below 1, an important threshold value of the crack density is that of percolation threshold, close to 0.1. Below this value, the rock permeability is 0. Close to 0.1, the percolative regime represents a transition between 0 and finite permeability. Above 0.1, the permeability is that of a connected regime where permeability can increase due to crack propagation. The implication is that permeability in deforming rocks (in the brittle or semi-brittle regimes) is not constant.

Acknowledgements

The authors thank M. Kachanov and T.-F. Wong for their careful reviews.

References

Anderson, D.L., Minster, B., Cole, D., 1974. The effect of oriented cracks on seismic velocities. J. Geophys. Res. 79, 4011–4015.

Ayling, M.R., Meredith, P.G., Murell, S.A.F., 1995. Microcracking during triaxial deformation of porous rocks monitored by changes in rock physical properties: I. Elastic-wave propagation measurements on dry rocks. Tectonophysics 245, 205–222.

Biot, M.A., 1956a. Theory of propagation of elastic waves in a fluid-saturated porous rock: I. Low frequency range. J. Acoust. Soc. Am. 28, 168–178.

Biot, M.A., 1956b. Theory of propagation of elastic waves in a fluid-saturated porous rock: II. Higher frequency range. J. Acoust. Soc. Am. 28, 168–178.

Brace, W.F., Walsh, J.B., Frangos, W.T., 1968. Permeability of granite under high pressure. J. Geophys. Res. 73, 2225–2236.

Brown, R.J.S., Korringa, J., 1975. On the dependence of the elastic properties of porous rock on the compressibility of the pore fluid. Geophysics 40, 608–616.

De Gennes, P.G., 1976. The Physics of Liquid Crystals. Oxford Univ. Press, New York.

Dienes, J., 1982. Permeability, percolation and statistical cracks mechanics. In: Goodman, R.E., Heuze, F.E. (Eds.), Rock Mechanics. American Institute of Mining, Metallurgical and Petroleum Engineers, New York, pp. 86–94.

Eshelby, J.D., 1957. The determination of the elastic field for an elliptical inclusion, and related problems. Proc. R. Soc. Lond., Ser. A 241, 376–396.

Fisher, G.J., Paterson, M.S., 1992. Measurement of permeability and storage capacity in rocks during deformation at high temperature and pressure. In: Evans, B., Wong, T.F. (Eds.), Fault Mechanics and Transport Properties of Rocks. Academic Press, San Diego, pp. 213–252.

Frisch, H.L., Hammersley, J.M., Welsh, D.J.A., 1962. Monte Carlo estimates of percolation probabilities for various lattices. Phys. Rev. 126, 949–951.

Gassmann, F., 1951. Uber die Elastizität poröser Medien. Vierteljahrschrift der Naturforschenden Gesellschaft in Zurich 96, 1–23.

Guéguen, Y., Dienes, J., 1989. Transport properties of rocks from statistics and percolation. Math. Geol. 21, 1–13.

Hudson, J.A., 1980. Overall properties of a cracked solid. Math. Proc. Camb. Philos. Soc. 88, 371–384.

Hudson, J.A., 1981. Wave speeds and attenuation of elastic waves in material containing cracks. Geophys. J. R. Astron. Soc. 64, 133–150.

Hudson, J.A., 1986. A higher order approximation to the wave propagation constants for a cracked solids. Geophys. J. R. Astron. Soc. 87, 265–274.

Kachanov, M., 1982. A microcrack model of rock inelasticity: Part II. Propagation of microcracks. Mech. Mater. 1, 29–41.

Kachanov, M., 1992. Effective elastic properties of cracked solids: critical review of some basic concepts. Appl. Mech. Rev. 45, 304–335.

Kachanov, M., 1993. Elastic solids with many cracks and related problems. Adv. Appl. Mech. 30, 259–445.

Kern, H., 1978. The effect of high temperature and high confining pressure on compressional wave velocities in quartz bearing and quartz free igneous and metamorphic rocks. Tectonophysics 44, 185–203.

Kern, H., 1982. Elastic wave velocities and constants of elasticity of rocks at elevated pressures and temperatures. Numerical Data and Functional Relationships, Landolt-Bornstein, New Ser., vol. 1b, pp. 99–140.

Kern, H., Liu, B., Popp, T., 1997. Relationship between anisotropy of P and S wave velocities and anisotropy of attenuation in serpentinite and amphibolite. J. Geophys. Res. 102, 3051–3065.

Le Ravalec, M., Guéguen, Y., 1996. High and low frequency elastic moduli for a saturated porous/cracked rock—differential self consistent and poroelastic theories. Geophysics 61, 1080–1094.

Le Ravalec, M., Guéguen, Y., Chelidze, T., 1996. Elastic wave velocities in partially saturated rocks: saturation hysteresis. J. Geophys. Res. 101, 837–844.

Madden, T.R., 1983. Microcrack connectivity in rocks: a renormalization group approach to the critical phenomena of conduction and failure in crystalline rocks. J. Geophys. Res. 88, 585–592.

Mavko, G., Jizba, D., 1991. Estimating grain-scale fluid effects on velocity dispersion in rocks. Geophysics 56, 1940–1949.

Mavko, G., Nur, A., 1975. Melt squirt in the asthenosphere. J. Geophys. Res. 80, 1444–1448.

Nye, J.F., 1979. Physical Properties of Crystals. Oxford Univ. Press, Oxford. 322 pp.

O'Connell, R., Budiansky, B., 1974. Seismic velocities in dry and saturated rocks. J. Geophys. Res. 79, 5412–5426.

O'Connell, R., Budiansky, B., 1977. Viscoelastic properties of fluid saturated cracked solids. J. Geophys. Res. 82, 5719–5736.

Peach, C., Spiers, C., 1996. Influence of crystal plastic deformation on dilatancy and permeability development in synthetic salt rock. Tectonophysics 256, 101–128.

Rivier, N., Guyon, E., Charlaix, E., 1985. A geometrical approach to percolation through random fractured rocks. Geol. Mag. 122, 157–162.

Sayers, C.M., Kachanov, M., 1991. A simple technique for finding effective elastic constants of cracked solids for arbitrary crack orientation statistics. Int. J. Solids Struct. 27, 671–680.

Sayers, C.M., Kachanov, M., 1995. Microcrack induced elastic wave anisotropy of brittle rocks. J. Geophys. Res. 100, 4149–4156.

Schubnel, A., Guéguen, Y., 2003. Dispersion and anisotropy in cracked rocks. J. Geophys. Res. 108, 2101–2116.

Schubnel, A., Nishizawa, O., Masuda, K., Lei, X.J., Xue, Z., Guéguen, Y., 2003. Velocity measurements and crack density determination during wet triaxial experiments on Oshima and Toki granites. Pure Appl. Geophys. 160, 869–888.

Scott, T.E., Ma, Q., Roegiers, J.C., 1993. Acoustic velocity changes during shear enhanced compaction of sanstone. Int. J. Rock Mech. 30, 763–769.

Simmons, G., Brace, W.F., 1965. Comparison of static and dynamic measurements of compressibility of rocks. J. Geophys. Res. 70, 5649–5656.

Simpson, G., Guéguen, Y., Schneider, F., 2001. Permeability enhancement due to microcrack dilatancy in the damage regime. J. Geophys. Res. 106, 3999–4016.

Soga, N., Mizutani, H., Spetzlet, H., Martin, R.J.I., 1978. The effect of dilatancy on velocity anisotropy in westerly granite. J. Geophys. Res. 83, 4451–4458.

Stauffer, D., Aharony, A., 1992. Introduction to Percolation Theory. Taylor and Francis, London. 181 pp.

Thomsen, L., 1985. Biot-consistent elastic moduli of porous rocks: the low frequency limit. Geophysics 50, 2797–2807.

Walsh, J.B., 1965. The effect of cracks on the compressibility of rock. J. Geophys. Res. 70, 381–389.

Wong, T.-F., David, C., Zhu, W., 1997. The transition from brittle faulting to cataclastic flow in porous sandstones: mechanical deformation. J. Geophys. Res. 102, 3009–3025.

Zhang, S., Cox, S.F., Paterson, M.S., 1994. The influence of room temperature deformation on porosity and permeability in calcite aggregates. J. Geophys. Res. 99, 761–775.

Zhu, W., Wong, T.-F., 1999. Network modeling of the evolution of permeability and dilatancy in compact rock. J. Geophys. Res. 104, 2963–2971.

Zoback, M.D., Byerlee, J.D., 1975. The effect of microcrack dilatancy on the permeability of westerly granite. J. Geophys. Res. 80, 752–755.